Research Square

Preprints are preliminary reports that have not undergone peer review.
They should not be considered conclusive, used to inform clinical practice,
or referenced by the media as validated information.

Identification of a distinct AREG+ cell population that promotes the progression, recurrence, and metastasis of endometrioid endometrial cancer at single-cell resolution

Wanwan Qi
Nanjing Medical University
Shuning Tian
Nanjing Medical University
Yiting He
Nanjing Medical University
Yuxuan Huang
Nanjing Medical University
Xueting Han
Nanjing Medical University
Tian Feng
Nanjing Medical University
Hongbiao Shen
Nanjing Medical University
Xinxia Chang
Nanjing Medical University
Hangzhou Xu
Nanjing Medical University
Yongfeng Tang
Nanjing Medical University
Zhenqin Feng
Nanjing Medical University
Qi Tang
Nanjing Medical University
Yun Gu
Nanjing Medical University
Huilin Zhang
Zhanghuilin068@njmu.edu.cn

Nanjing Medical University

Article

Keywords: AREG, endometrial cancer, endometrioid endometrial cancer, peritumoral tissue, single-cell RNA sequencing

Posted Date: February 27th, 2026

DOI: https://doi.org/10.21203/rs.3.rs-8692432/v1

License: This work is licensed under a Creative Commons Attribution 4.0 International License. Read Full License

Additional Declarations: No competing interests reported.

Abstract

Endometrial cancer (EC) is the second most common malignant tumor of the female reproductive system worldwide. Endometrioid endometrial cancer (EEC) constitutes the most prevalent subtype, representing approximately 75% of all EC cases. Most patients diagnosed with EEC present at an early stage and generally exhibit a favorable prognosis. However, a small subset of low-grade, early-stage, well-differentiated EECs may exhibit metastatic behavior and recurrence. Early alterations in the microenvironment of the peritumoral region, particularly concerning the proliferation, migration, and invasion of tumor cells within this area, are critical factors influencing tumor progression, metastasis, and recurrence. In this study, single-cell RNA sequencing (scRNA-seq) technology was used to sequence five EEC tumors and four peritumoral tissues from patients diagnosed with early-stage EEC. For the first time, a population of cells exhibiting high expression of AREG was identified in the peritumoral region of EECs. Bioinformatics analyses revealed that this population of cells demonstrated significant capabilities for proliferation, migration, and invasion. The immunohistochemistry (IHC) analysis of the tissue microarray (TMA) revealed elevated AREG expression in EECs, which correlated with various clinical parameters, including FIGO stage, degree of differentiation, pelvic lymph node metastasis, muscular layer infiltration, Ki67 expression, and PAX-2 expression. Both *in vitro* and *in vivo* experiments confirmed that AREG promotes malignant biological behaviors in EECs, including proliferation, migration, invasion, and regulation of apoptosis and the cell cycle. Additionally, AREG was found to activate the EGFR-Smad2/3 signaling pathway through phosphorylation, inducing epithelial-mesenchymal transition (EMT) and thus promoting the migration and invasion abilities of EECs. This study identified a high AREG-expression cell population in EECs, providing valuable insights into the pathological mechanisms of EEC progression, recurrence, and metastasis, and proposing AREG as a potential biomarker for the prognostic prediction and targeted therapeutic strategies in EECs.

1. Introduction

Endometrial cancer (EC) is the second most common malignant tumor of the female reproductive system worldwide, with a particularly high incidence in North America and Eastern Europe[1]. It is more commonly diagnosed in women during the perimenopausal and postmenopausal stages[2]. In recent years, the incidence and mortality rates of EC have been increasing annually, with a notable trend toward younger age at diagnosis[3]. According to the National Cancer Centre in 2022, the incidence rate of EC in China was 11.25/100 000, with a mortality rate of 1.96/100 000, showing an increasing trend in both incidence and mortality, alongside a shift toward younger age at first diagnosis. The main pathological types of EC include endometrioid endometrial cancer (EEC), serous cancer, and clear-cell cancer. Among them, EEC is the most common, constituting approximately 75% of all cases[4]. The Cancer Genome Atlas (TCGA) classified EC into four molecular subtypes: (1) POLE ultra-mutated, (2) microsatellite instability hypermutated, (3) low copy number, and (4) high copy number[5]. Most patients are diagnosed with EEC at an early stage and have a favorable prognosis. However, a minority of low-grade, early-stage, well-differentiated EECs may metastasize and recur. This subset often exhibits a high degree of somatic

copy number variations (CNVs)[6]. These patients often have a poor prognosis due to the lack of specific targeted therapeutic options. Therefore, there is an urgent need for further exploration of the molecular mechanisms of metastasis and recurrence of highly aggressive EEC and identification of molecular targets for early diagnosis, prognostication and precision targeted therapies of EEC.

Since its first report in 2009, single-cell RNA sequencing (scRNA-seq) technology has gained widespread application within the life sciences[7]. Its emergence and development have played important roles in elucidating the mechanisms of tumor initiation and progression, identifying rare cells, mapping cell lineages, guiding targeted precision therapies, and predicting patient prognosis.

The peritumoral region plays a crucial role in facilitating dynamic interactions between tumor cells and their surrounding cells. Early alterations in the microenvironment of the peritumoral region, particularly concerning the proliferation, migration, and invasion of tumor cells, play crucial roles in tumor progression, metastasis, and recurrence[8, 9]. As our understanding of tumorigenesis and tumor development expands, there is an increasing recognition of the importance of studying the peritumoral region. However, comprehensive investigations into tumor cells in the peritumoral region of EEC are limited.

This study intends to employ scRNA-seq technology to explore the microenvironment of early-stage EEC, especially the peritumoral region, thus identifying tumor cells with invasive, metastatic and recurrent potential. Additionally, it seeks to explore the influence of relevant tumor cells on EEC metastasis and recurrence and molecular mechanisms through EEC tissue microarrays, *in vitro* cellular experiments and construction of animal models *in vivo*. This study aims to elucidate novel molecular mechanisms leading to the metastasis and recurrence of EEC, and to identify molecular targets for early diagnosis, prognosis and precision targeted therapy of EEC.

2. Results

2.1 Cellular atlas of EEC and peritumoral tissues

Six paired samples of human EEC tumor and peritumoral samples obtained by surgical resection were dissociated and prepared into single cell suspensions. After single-cell transcriptome library preparation, the number of cells, median UMI, saturation and other library parameters were quantified. The final scRNA-seq analysis was conducted on 5 tumor samples and 4 paired peritumoral samples, as depicted in Fig. 1A. After quality control to exclude low-quality data, a total of 64 482 transcriptome datasets from cells were obtained for further bioinformatics analysis. Among them, 39 857 cells were derived from tumor tissues, whereas 24 625 cells were derived from peritumoral tissues. After removing batch effects, unsupervised clustering analysis was performed on EEC and peritumoral cells. 10 cellular subpopulations were identified using canonical gene markers and copy number variation (CNV) analysis with EC denoting tumor samples and ECP denoting peritumoral samples (Fig. 1B). EEC is a malignant tumor that originates from the glandular epithelium. Glandular epithelial cells exhibiting high CNV are

often associated with poor prognosis and an increased risk of recurrence. CNV analysis was performed on all epithelial cells derived from both tumor and peritumoral tissues to identify malignant epithelial cells. The results revealed that, compared to control cells (including myeloid cells, plasma cells, and T cells), chromosomal amplifications in epithelial cells were predominantly located on chromosomes 1, 3, and 7, whereas deletions were observed on chromosome 12 (Figure S1A). Based on CNV scores cancer-specific marker genes, we identified 15 965 epithelial cancer cells and 24 025 epithelial normal cells. The UMAP projection revealed the distribution of epithelial cancer cells and epithelial normal cells across different samples (Figure S1B, Figure S1C). Due to the lack of tumor tissue from Patient 4 and the absence of epithelial cancer cells in the corresponding peritumoral tissue, data related to ECP4 were excluded from the subsequent study of epithelial cancer cells to minimize the likelihood of chance findings and maintain the robustness of the results. The proportions of the 10 cell types varied greatly among the different samples, suggesting the heterogeneous characteristics of the TME in EEC (Fig. 1B). Cancer cells were predominantly distributed in tumor tissues, consistent with established understanding. However, a small proportion cancer cells are still distributed in the peritumoral area. The feature plot illustrates the marker genes of the 10 cellular subpopulations (Fig. 1C). The top 6 differentially expressed genes for each cell type are illustrated in violin plots (Fig. 1D).

2.2 Distinct features of epithelial cancer cells in EEC and peritumoral tissues

Epithelial cancer cells were classified into three subtypes based on specific gene expression profiles and gene set variation analysis (GSVA) to gain a better understanding of the intrinsic characteristics of epithelial cancer cells: Subtype 1 (S1), Subtype 2 (S2), and Subtype 3 (S3). Notably, S3 was predominantly composed of epithelial cancer cells derived from peritumoral samples (Fig. 2A). A significant difference in the distribution of S3 cells were observed between the tumor and peritumoral samples. Nevertheless, cells from the other subtypes exhibited extreme heterogeneity among the groups, with varying distributions and no significant differences (Fig. 2B).

In the next step, an analysis of differentially expressed genes was performed, and representative genes that were highly expressed in each subtype were identified (Fig. 2C). The characteristic gene expression profiles of these representative genes were as follows: S1: AKR1C3, SPP1; S2: LCN2, AOC1; S3: AREG, IGF2BP2 as depicted in Fig. 2E. GSVA revealed that S1, S2, and S3 were functionally engaged in energy metabolism, tumorigenesis, tumor proliferation and metastasis, respectively (Fig. 2D). The classical genes associated with active pathways in the three subtypes exhibited high expression levels within their respective subtypes[10–17] (Fig. 2F). Combining the results of differential gene expression analysis and the classical genes of the relevant pathways, these three subtypes were designated as the $AKR1C3^{+}$ S1, $LCN2^{+}$ S2 and $AREG^{+}$ S3 cell populations, respectively. Then we conducted a CNV analysis across these three subtypes, utilizing normal epithelial cells as a control (Figure S1D). The findings further substantiated that these three subgroups were classified as malignant epithelium, with the $AREG^{+}$ S3 and the $LCN2^{+}$S2 exhibiting a higher degree of malignancy compared to the $AKR1C3^{+}$ S1 (Figure S1E-S1F).

Given the unique distribution characteristics of S3 cells, particular emphasis was placed on the attributes of the AREG$^+$ S3 cell population. AREG$^+$ S3 also attracted significant interest because of its enriched functions, including the activation of cancer-related pathways, particularly those associated with the epithelial-mesenchymal transition (EMT). Moreover, AREG$^+$ S3 exhibited strong associations with the regulation of apoptosis, the cell cycle, and angiogenesis. These observations align with the functional attributes of the highly expressed representative genes within AREG$^+$ S3, including AREG, IGF2BP2, UCA1, NRP2, ARL4C, and EMP1.

2.3 Functional identification and analysis of the AREG$^+$ S3 cell population

To validate the accuracy and robustness of the results obtained for the three subtypes derived from GSVA, gene set enrichment analysis (GSEA) was conducted to confirm the findings independently (Fig. 3A, Figure S2A). The results showed that gene sets related to DNA repair and oxidative phosphorylation were enriched in AKR1C3$^+$ S1, tumor stemness related gene sets were enriched in LCN2$^+$ S2, and EMT and cell proliferation related gene sets were enriched in AREG$^+$ S3. Cell proliferation-related genes MKI67, AREG, EMP1, CCND1 and EMT-related genes FN1, AREG, IGF2BP2, FBN2 were highly expressed in AREG$^+$ S3 (Fig. 3B).

The cell cycle phases of the three subtypes were inferred using the "Cell Cycle Scoring" function (Fig. 3C-3D). The results revealed that AREG$^+$ S3 had significantly higher proportion of S and G2M phases. Moreover, the proportion of S and G2M phases of AREG$^+$ S3 in ECP were higher than that in cancer tissues. This indicated that AREG$^+$ S3 has a strong potential for proliferation and differentiation. A SLICE entropy analysis of stemness was performed on the three subtypes, revealing that AREG$^+$ S3 displayed stronger tumor stemness. Furthermore, the expression of stemness-related genes, such as KLF5 and MYC, was predominantly concentrated in AREG$^+$ S3 (Fig. 3E).

We performed SCENIC (Single cell regulatory network inference and clustering) analysis to reveal potential transcription factors (TFs) underlying the regulation across subtypes at the single-cell level (Fig. 3F). Metabolism-related TFs such as XBP1 were enriched in AKR1C3$^+$ S1. Genes involved in tumorigenesis such as ZBTB7B and KLF8 were upregulated in LCN2$^+$ S2. Meanwhile, the expression of FOSL1 and ZEB1, which were associated with tumor proliferation and migration, was significantly increased in AREG$^+$ S3.

A refined pseudo-time analysis was conducted with Monocle2 to delve into the potential evolutionary relationships among the three subtypes. As depicted in Fig. 3G, LCN2$^+$ S2 was identified at the origin of the evolutionary process, with AREG$^+$ S3 positioned at the commencement and intermediate phases of cell evolution. Meanwhile, the AKR1C3$^+$ S1 was observed to be situated at the terminal stage of the evolutionary trajectory. We also observed that genes related to tumor proliferation and metastasis, such as AREG and UCA1, were upregulated at the beginning and intermediate stages of the trajectory and

downregulated in the latter stages (Fig. 3H). Genes displaying the most significant changes in expression over time were classified into five major clusters via hierarchical clustering. EFCAB1, LRRC23, SPA17, and WDR54 in Cluster 5 were up-regulated in the terminal state, and this expression profile significantly overlapped with the characteristic genes of AKR1C3$^+$ S1 (Fig. 3I).

2.4 Cell-cell communication between three subtypes and other cell types

The immunological scoring results for the three subtypes revealed that AKR1C3$^+$ S1 exhibited elevated scores for cytokines, LCN2$^+$ S2 demonstrated higher scores for chemokines, and AREG$^+$ S3 showed higher scores for immune checkpoints (Fig. 4C).

The CellPhoneDB ligand-receptor complex database was subsequently utilized to predict ligand-receptor pairs between the three subtypes and nine other cell types (Fig. 4B). The findings revealed that the three subtypes displayed enhanced interactions with T cells, macrophages, and fibroblasts (Fig. 4A). In the peritumoral region, AREG$^+$ S3-ECP generated a greater number of ligand-receptor pairs with other cells compared to the LCN2$^+$ S2-ECP (Fig. 4A).

Next, an analysis was conducted on the 12 most significantly differentially expressed ligands in cancer cells to evaluate the variations in crosstalk between Subtype 1–3 EC/ECP and other cell types (Fig. 4D, Figure S3A). Among these ligands, the gene MIF, which exhibited elevated expression in AKR1C3$^+$ S1-EC, demonstrated a strong interaction with CD74 on dendritic cells (DCs), monocytes, and macrophages. The AKR1C3$^+$ S1-ECP exhibited close communication with monocytes, macrophages, and DCs. Additionally, LGALS9-HAVCR2 and SAA1-FPR2 showed pronounced interactions. The ligand TNFSF10, also referred as tumor necrosis factor-associated apoptosis-inducing ligand, interacted with TNFRSF10B and RIPK1 in LCN2$^+$ S2-EC/ECP. Given that AREG$^+$ S3 cells were predominantly localized in the peritumoral region, our investigation primarily concentrated on the AREG$^+$ S3-ECP fraction, and we found that CCL5-CCR1, ANXA1-FPR2 and ANXA1-FPR3 exhibited functional activity. Special emphasis was placed on the highly expressed ligand MDK, which is a heparin-binding growth factor. Its receptor, LRP1, is expressed on DCs, monocytes, and macrophages. The relative expression level of the aforementioned key genes are presented in Fig. 4E. Furthermore, the influence of other cell-derived cytokines on AREG$^+$ S3 cells were explored, as depicted in Figure S3B-S3C.

2.5 AREG expression in EEC tissues and peritumoral tissues and its relationship with the clinicopathological factors and prognosis

A comprehensive analysis was conducted by comparing the gene set (S1-S3) with the expression data from the bulk transcriptome of clinical samples obtained from the TCGA-EEC database. This analysis aimed to elucidate the relationship between the scRNA-seq data and clinical EEC cases. These results revealed a significant impact of the gene set associated with AKR1C3$^+$ S1 and LCN2$^+$ S2 on the patient

prognosis (Fig. 5A). Furthermore, the gene set related to AREG$^+$ S3 gradually increased across various stages of EEC, with notable prominence in stages I and III (Fig. 5B).

We collected tumors and peritumoral tissues from 296 EEC patients at the Affiliated Obstetrics and Gynecology Hospital of Nanjing Medical University to explore the potential correlation between AREG protein expression and clinicopathological factors of EEC patients. These tissues were used to create tissue microarrays (TMAs), which were then subjected to immunohistochemical (IHC) staining using specific antibodies targeting AREG and PAX-2. The IHC analysis revealed that AREG protein was expressed mainly in the cell membrane and cytoplasm, while PAX-2 protein was expressed mainly in the nucleus. AREG exhibited high expression levels in EEC tissues, contrasting with low or absent expression in normal endometrial epithelial tissues. Conversely, PAX-2 was expressed at low levels or absent in EEC tissues, while exhibiting high levels in normal endometrial epithelial tissues (Fig. 5C). The positive expression rates of AREG in EEC stages I, II and III were recorded at 62.8% (147/234), 70.3% (26/37) and 88% (22/25), respectively, indicating a positive correlation between the expression of AREG and FIGO stage, with a statistically significant difference ($P < 0.05$) (Fig. 5D).

In EEC tissues, the expression of AREG was analyzed in relation to the clinicopathological factors of 296 patients by the χ^2 test. The results revealed that elevated levels of AREG protein in EEC tissues were associated with several clinical parameters, including FIGO stage ($\chi^2 = 6.733$, $P = 0.035$), differentiation degree ($\chi^2 = 10.098$, $P = 0.006$), pelvic lymph node metastasis ($\chi^2 = 5.298$, $P = 0.021$), myxoid infiltration ($\chi^2 = 5.782$, $P = 0.021$), Ki67 expression ($\chi^2 = 4.873$, $P = 0.027$), and PAX-2 expression ($\chi^2 = 17.556$, $P < 0.001$). Conversely, no significant associations were found between AREG expression and factors such as age, abdominal lymph node metastasis, ER expression, PR expression, PTEN expression, or P53 expression (S Table 2). In EEC paired peritumoral tissues, due to the infiltration of EEC into the myometrium, endometrial epithelial tissues were observed in only 16 samples. Among these, AREG-positive malignant epithelial cells were identified, with a positive high expression rate of 62.5% (10/16) (Fig. 5E).

At the mRNA level, data from TIMER2.0 revealed that the expression of AREG was elevated in tumor tissues compared to normal tissues, whereas the expression of PAX-2 was found to be higher in normal tissues than in tumors (Figure S4A). Data from the OncoLnc database revealed that patients exhibiting high levels of AREG expression experienced shorter survival times and poorer prognoses. In contrast, patients with elevated PAX-2 expression demonstrated longer survival times and better prognoses, but these differences were not statistically significant ($P > 0.05$) (Figure S4B).

Given the significant differentiation potential observed in S3, we sought to investigate whether AREG might also contribute to EEC formation. To address this, we collected tissue sections from nine normal endometrial epithelial samples, nine atypical endometrial hyperplasia (AEH) samples, and nine EEC samples for subsequent IHC staining analysis. The findings showed that the AREG H-SCOREs for normal endometrial epithelial tissues, AEH, and EEC were 118.9 ± 28.48, 207.8 ± 31.14, and 248.3 ± 47.70 points, respectively, with statistically significant differences ($P < 0.05$). In contrast, the PAX-2 H-SCOREs were

182.2 ± 72.07, 102.2 ± 47.64, and 28.89 ± 39.83, respectively, with statistically significant differences ($P < 0.05$) (Figure S4C-S4D).

2.6 Effects of AREG on the biological behaviors of EEC cells *in vitro*

We established stable transfected cell lines exhibiting AREG knockdown and overexpression using lentiviral vectors to explore the potential role of AREG in EEC development. The expression levels of AREG in human EEC cell lines and normal endometrial epithelial cells (HNEECs) were examined at the mRNA and protein levels using reverse transcription quantitative polymerase chain reaction (RT-qPCR) and western blot (WB) assays, respectively. Notably, AREG was found to be highly expressed in the EEC cell lines HEC-1-A and ISHIKAWA, while its expression was comparatively lower in the EEC cell lines MFE 296, AN3 CA and HNEECs (Figure S5A-S5B). The sh-Control and sh-AREG lentiviruses were transfected into the ISHIKAWA cell line with high AREG expression levels, and the AREG-VE and AREG-OE lentiviruses were transfected into the AN3 CA cell line with low AREG expression levels. Following a screening period exceeding two weeks, stable cell lines with AREG-knockdown and overexpression were successfully constructed. The efficiencies of AREG knockdown and overexpression were subsequently evaluated using RT-qPCR, WB, and flow cytometry (FCM) (Figure S5C-S5D).

We assessed the impacts of AREG on cellular proliferation using 5-ethynyl-2' -deoxyuridine (EdU), cell counting kit-8 (CCK-8), and colony formation assays. The results revealed a notable reduction in the proliferation rate of cells within the ISHIKAWA-sh-AREG group compared to the ISHIKAWA-sh-Control group. Conversely, the AN3 CA-AREG-OE group exhibited a significant enhancement in cell proliferation relative to the AN3 CA-AREG-VE group (Fig. 6A-6C).

Subsequently, we conducted wound healing and transwell assays to investigate the impacts of AREG on cell migration. The results revealed a significant decrease in cell migration in the ISHIKAWA-sh-AREG group compared to the ISHIKAWA-sh-Control group, whereas the AN3 CA-AREG-OE group exhibited a pronounced increase in cell migration when compared to the AN3 CA-AREG-VE group (Fig. 6D-6E).

Annexin V-Alexa Fluor 647/PI staining, followed by FCM analysis, was performed to evaluate whether AREG affects the apoptosis of EEC cells. The results revealed a higher proportion of apoptotic cells in the ISHIKAWA-sh-AREG group compared to the ISHIKAWA-sh-Control group. Conversely, compared with the AN3 CA-AREG-VE group, the AN3 CA-AREG-OE group presented a significant reduction in the number of apoptotic cells (Fig. 6F). An FCM analysis of the cellular DNA content was subsequently conducted to evaluate the impact of AREG on cell cycle progression. Compared to the ISHIKAWA-sh-Control group, the proportion of S-phase cells was significantly decreased, and the proportion of G1-phase cells was significantly increased in the ISHIKAWA-sh-AREG group. Conversely, compared to the AN3 CA-AREG-VE group, the proportion of S-phase cells was significantly increased, and the proportion of G1-phase cells was significantly decreased in the AN3 CA-AREG-OE group (Fig. 6G).

2.7 Effects of AREG on EEC cell proliferation *in vivo*

A subcutaneous xenograft tumor model was established in BALB/c nude mice to further explore the impact of AREG on cellular proliferation *in vivo*. Compared to the ISHIKAWA-sh-Control group, the ISHIKAWA-sh-AREG group presented reduced tumor volumes and weights. Conversely, the AN3 CA-AREG-OE group presented increased tumor volumes and weights relative to the AN3 CA-AREG-VE group (Fig. 7A-7C). The tumors were subsequently subjected to immunofluorescence (IF) staining. This analysis involved colocalizing red-fluorescent AREG with green-fluorescent Ki67 in the tumor cells of both the AREG-knockdown and AREG-overexpressing tumor samples. The analysis revealed that the number of tumor cells stained for the proliferation marker Ki67 was lower in the ISHIKAWA-sh-AREG group than in the ISHIKAWA-sh-Control group, whereas the AN3 CA-AREG-OE group presented an increased number of tumor cells compared to the AN3 CA-AREG-VE group (Fig. 7D).

2.8 AREG induced the EMT via EGFR-Smad2/3 signaling to promote the migration and invasion of EEC cells

According to predictions derived from GSEA regarding pathway activity in both tumoral and peritumoral regions, the $AREG^{+}S3$ subtype exhibited activation of the EMT and TGFβ signaling pathways (Fig. 8A). Combined with existing literature, we speculated that AREG may promote the migration and invasion of EEC cells by activating the EGFR-Smad2/3 signaling pathway, consequently leading to the EMT (Fig. 8E). Pearson's correlation analysis utilizing the TIMER 2.0 database revealed a positive correlation between AREG and the mRNA expression levels of vimentin (VIM), N-cadherin (CDH2), SNAI2, and ZEB1 ($P < 0.0001$) (Fig. 8B). The relevant proteins of the EGFR-Smad2/3 signaling pathway were detected by WB, and the levels of both p-EGFR and p-Smad2/3 proteins were significantly downregulated when AREG was knocked down, whereas the overexpression of AREG lead to their upregulation (Fig. 8C). In addition, the EMT-related proteins were also detected, and the results revealed that the AREG-knockdown cell line presented increased expression of the E-cadherin protein and attenuated expression of the vimentin, N-cadherin, SNAI2, and ZEB1 proteins, whereas the AREG-overexpressing cell line presented the opposite results (Fig. 8D). The above experiments demonstrated that AREG promotes EEC cell migration and invasion by activating the EGFR-Smad2/3 signaling pathway, thereby promoting EMT.

3. Discussion

Although the majority of EECs have a favorable prognosis, a minority of tumors, specifically those characterized by a low-grade, early-stage, and well-differentiated cells, can exhibit recurrence and metastasis, unfortunately leading to a poor prognosis for these patients. As the understanding of tumorigenesis and development continues to advance, research is expanding beyond the study of the tumor ecosystem itself. A growing emphasis on investigating the ecosystems in the neighboring regions surrounding the tumor has been noted. In previous scRNA-seq studies on EC, the focus was mainly on the exploration of EC tissues and normal tissues[18–22]. These previous studies have improved our understanding of the pathogenesis and cellular characteristics of EC by analyzing EC tissues and normal tissues at the single-cell level. However, it cannot be ignored that as an important part of the tumor microenvironment, peritumoral tissues may play a key role in the occurrence, development and

metastasis of tumors. Nevertheless, they have been neglected in past research. In this study, scRNA-seq was conducted on five primary EEC tissues and four peritumoral tissues sourced from six patients diagnosed with early-stage EEC. By conducting a comprehensive analysis of the scRNA-seq data, we successfully generated a cellular map delineating EECs and their surrounding peritumoral regions, which facilitated the identification of specific subtypes of malignant cells that contribute to the progression, recurrence, and metastasis of EEC.

This study identified three distinct subtypes that are associated with various facets of EEC. These include the AKR1C3^{+} S1, which is linked to EEC resistance, the LCN2^{+} S2, which is associated with EEC formation, and the AREG^{+} S3, which is capable of promoting the malignant progression, metastasis, and recurrence of EEC. Interestingly, the AREG^{+} S3 was predominantly located in peritumoral regions. The S1 exhibited high expression levels of genes such as AKR1C3 and SPP1, which are closely related to oxidative phosphorylation and DNA repair[23, 24]. The genes that were highly expressed in the S2, including LCN2[20, 25] and OLFM4[26], are associated with tumorigenesis. In contrast, the S3 is characterized by elevated expression of genes such as AREG, IGF2BP2, UCA1, and NRP2, all of which are involved in tumor progression and metastasis. AREG, a ligand for epidermal growth factor receptor (EGFR), has been reported to play a significant role in promoting the proliferation, migration, and invasion of various types of cancers[27–30]. IGF2BP2, an N6-methyladenosine reader, interacts with multiple RNA species and correlates with poor prognosis in AML when overexpressed[31]. UCA1, an oncogenic noncoding RNA of more than 200 nucleotides in length, regulates key biological processes critical to cancer progression, including cell growth, invasion, migration, metastasis, and angiogenesis. Notably, UCA1 has been shown to promote the development of EC by regulating the expression of the KLF5 and RXFP1 genes[32]. NRP2, a member of the neurofibrillary protein family, is upregulated in tumor-associated macrophages and promotes tumor growth by regulating cytokinesis and immune responses within tumor cells[33].

Our bioinformatics analyses of AREG^{+} S3 revealed several important findings. First, this subtype possesses a strong potential for cellular differentiation and proliferation. The results of GSEA and entropy stemness analyses revealed that the tumor cells of S3 exhibited strong stemness characteristics. These properties significantly influence EEC maintenance, progression, and metastatic potential.. Second, the activation of multiple cancer-related pathways was observed within this subtype. Moreover, the genes that were highly expressed in AREG^{+} S3, along with their upstream transcription factors, were previously reported to play critical roles in promoting proliferation, migration, invasion, and angiogenesis in various tumor types. Notably, transcription factors ZEB1 and FOSL1 showed elevated expression in S3 ECP compared to S3 EC (Fig. 3H). Moreover, a correlation was observed between the expression levels of AREG and ZEB1 and FOSL1, as shown in Figure S2B. Previous studies have indicated that ZEB1 can transcriptionally activate PFKM, thereby enhancing the Warburg effect and promoting the progression and metastasis of hepatocellular carcinoma (HCC)[34]. Similarly, FOSL1 has been implicated in promoting the metastasis of head and neck squamous cell carcinoma stem cells

through a transcriptional program driven by super-enhancers[35]. In summary, these findings highlight the potential significance of AREG$^+$ S3 in the progression, metastasis, and aggressiveness of EEC.

The interaction between AREG$^+$ S3 and adjacent cell types through various ligand-receptor pairs plays crucial roles in the progression, recurrence, and metastasis of EEC. These findings suggest that the active ligand-receptor pairs, specifically CCL5-CCR1, ANAX1-FPR2/3, and MDK-LRP1, significantly influence the development of an immunosuppressive microenvironment in the peritumoral region of EECs. Such interactions may further contribute to the malignant progression of EEC. In the context of S3-ECP, previous studies have showed that the interactions between CCL5 and CCR1, as well as ANXA1 and FPR2/3, could promote the migration and invasion of cancer cells[36, 37]. Additionally, MDK is recognized as a critical regulator supporting the growth, survival, migration, and angiogenesis of various tumors[38]. Previous studies on EC revealed that EC cells can induce a malignant phenotype in endothelial cells through MDK-NCL signaling pathways. This signaling mechanism is linked to the suppression of immune responses, ultimately contributing to the development of an immunosuppressive TME[39]. Additionally, elevated levels of MDK could lead to its interaction with the receptor LRP1 on tumor-infiltrating macrophages in gallbladder cancer. This interaction promotes the differentiation of immunosuppressive macrophages, potentially contributing to the suppression of immune responses within the TME. Furthermore, increased MDK expression has been linked to reduced overall survival of patients with gallbladder cancer[40]. Therefore, we hypothesize that MDK on S3-ECP binds to LRP1 on DCs, monocytes, and macrophages, fostering an immunosuppressive microenvironment and consequently driving the malignant progression of EEC. Based on the predicted of ligand-receptor interactions between AREG$^+$ S3 and other cells in the surrounding microenvironment, we propose that AREG, which drives the malignant progression of EEC, may originate from epithelial cells, DCs and fibroblasts. Indeed, previous studies have demonstrated that DC-derived AREG promotes the malignant progression of lung cancer[29]. Moreover, lysophosphatidic acid has been shown to stimulate cancer-associated fibroblasts to secrete increased levels of AREG, thereby enhancing cancer cell invasiveness and metastasis[41]. These findings support our hypothesis that interactions between AREG$^+$ S3 and DCs or fibroblasts may also contribute to the aggressive behaviors of EEC. However, further experimental validation is required to confirm these hypotheses.

To validate the bioinformatic findings, we integrated our own set of key genes from AREG$^+$ S3 into TCGA-EEC database for subsequent analysis. Interestingly, a slight upregulation of these genes was observed within EEC stages I-III. Given the predominant localization of S3 in peritumoral regions and its strong association with EEC progression, recurrence, and metastasis in functional analyses, we focused on experimentally validating the role of S3 in EEC. AREG exhibited high expression in S3, especially in peritumoral regions (Fig. 3B). Additionally, previous research has consistently indicated that AREG plays vital roles in promoting the proliferation, migration, and invasion of various tumor types. Therefore, AREG was selected as a representative gene of S3 for our subsequent experimental investigation.

In order to further verify the expression of AREG in EEC tissues and peritumoral tissues at the protein level, and investigate its association with clinicopathological factors and prognosis, this study collected EEC tissues and paired peritumoral tissues from 296 surgical EEC patients for TMA analysis and performed IHC staining for AREG and PAX-2. PAX-2 is known to be significantly involved in the development of various organs, including the kidney, thyroid, male testes, epididymis, female uterus, and fallopian tubes. In adult females, the PAX-2 protein is expressed predominantly in the nuclei of the glandular epithelium in normal endometrial tissues. However, its expression is either diminished or absent in the glandular epithelium of some patients with endometrial intraepithelial neoplasia and is further reduced or absent in EC[42]. TMA results revealed an increasing trend in AREG protein expression across EEC stages I-III. In addition, peritumoral regions in early EEC samples contained $AREG^+$ cells with potentially malignant features, consistent with our previous scRNA-seq findings of a malignant epithelial cell population with high AREG expression in peritumoral regions. However, due to the technical limitations in sampling and muscular layer infiltration, endometrial epithelial tissues were observed in only a small number of peritumoral tissues. Analysis of the clinicopathological features and expression of AREG in 296 EEC patients revealed that elevated AREG expression in EECs was associated with advanced FIGO stage, poorer differentiation, increased pelvic lymph node metastasis, deeper myometrial infiltration, higher expression of Ki67, and lower expression of PAX-2, indicating the close association between high AREG expression and malignant progression and metastasis in EEC. Furthermore, our data revealed a progressive increase in the expression of AREG from normal tissue to AEH to EEC, indicating its potential role in the formation of EEC. Based on the above findings, AREG is a promising biomarker for early diagnosis, prognostic guidance and precision targeted therapy of EEC.

The follow-up time of 296 patients was 60 months, and since some patients had not yet reached the follow-up time; however, as some patients had not yet reached this time point, the analysis of AREG expression and its correlation with prognosis in these EEC patients remains incomplete and will be finalized in subsequent analyses. Correlation analyses were performed using data from the TCGA database to investigate the relationship between the expression of AREG and PAX-2 and the prognosis of EEC patients. However, the results revealed no statistically significant difference. The reason for this may be that the prognosis for EEC is generally good compared to that for other tumors.

In vitro and *in vivo* experiments showed that AREG promoted malignant biological behaviors, such as EEC proliferation, migration and invasion and regulating EEC apoptosis and the cell cycle. We further explored the mechanism underlying AREG-mediated promotion of EEC migration and invasion, and GSEA revealed that AREG might be associated with the TGFβ and EMT signaling pathways. In the TGFβ signaling pathway, Smad2/Smad3 are considered key mediators[43]. EMT is an important cellular program that confers the metastatic potential to tumor cells during tumor formation and progression[44]. At the mRNA level, AREG expression was positively correlated with the expression of the EMT associated proteins, including vimentin, N-cadherin, SNAI2 and ZEB1. At the protein level, the WB results suggested that AREG promoted the migration and invasion of EEC cells by promoting the phosphorylation of proteins in the EGFR-Smad2/3 signaling pathway, leading to EMT.

Recent studies have confirmed that TGFβ derived from malignant pancreatic ductal adenocarcinoma (PDAC) cells was able to induce the autocrine secretion of AREG in myofibroblast carcinoma-associated fibroblasts (myCAFs), which further activated the EGFR/ERBB2 signaling pathway, enhancing the metastatic potential of PDAC cells[45]. These findings suggest that TGFβ induces the expression of AREG, thereby activiting downstream pathway, but the specific mechanism of action between TGFβ and AREG requires further investigation.

This study is subject to certain limitations, notably the limited sample size of patients included in the study, which may not adequately reflect the broader population of individuals with EEC. Therefore, future studies should aim to utilize a larger cohort and implement multi-sample co-analysis using additional scRNA-seq data. Furthermore, both *in vitro* and *in vivo* experiments are necessary to corroborate the results derived from bioinformatics analyses. Such approaches will further enhance the validity and dependability of our findings.

In summary, this study utilized scRNA-seq to analyze five tumor samples and four peritumoral samples from patients diagnosed with early-stage EEC. A malignant epithelial cell population characterized by elevated expression of AREG was identified for the first time in the peritumoral region of EEC. These cells exhibit strong capabilities in terms of proliferation, migration, and invasion, which are critical factors in the progression, metastasis, and recurrence of EEC. The expression of AREG is notably high in EEC and correlates with various clinical parameters, including the FIGO stage, differentiation, pelvic lymph node metastasis, myometrial invasion, Ki67 expression, and PAX-2 expression. This correlation indicates that AREG is intricately linked to the malignant progression and metastasis of EEC. Furthermore, AREG promotes malignant biological behaviors in EEC, including proliferation, migration, invasion, and regulation of apoptosis and the cell cycle. It activates the EGFR-Smad2/3 signaling pathway through phosphorylation, which induces EMT and enhances the migration and invasion abilities of EEC cells. These findings provide valuable insights into the pathological mechanisms of EEC progression, metastasis and recurrence, and they suggest potential applications for prognostic prediction and targeted therapeutic strategies. AREG is anticipated to serve as a molecular target for early diagnosis, prognostic evaluation, and precision targeted therapy in EEC.

4. Materials and methods

Human subjects

This study enrolled a total of 6 EEC patients, aged between 45 and 68 years, with a mean age of 56.3 years. The clinicopathological data of the 6 patients are presented in S Table 1. None of the patients had received chemotherapy, radiotherapy, or immunotherapy prior to surgery. The pathological stages of the 6 EEC patients were determined according to the FIGO 2023 criteria for endometrial cancer staging, with 4 patients classified as stage Ia, 1 as stage Ib, and 1 as stage II. The endometrial samples were surgically excised at the Affiliated Obstetrics and Gynecology Hospital of Nanjing Medical University between January and June 2021. For each patient, one tumor sample and one peritumoral sample

(located ≥ 2 cm away from the tumor margin) were collected for scRNA-seq analysis. The tumor tissue from patient No. 4 did not meet the quality criteria for single-cell sequencing, and thus was therefore excluded from further processing. For patients No. 3 and No. 6, peritumoral tissues could not be collected due to the extensive size of their tumor tissues. A total of 5 tumor tissue samples and 4 peritumoral tissue samples were obtained and pathologically confirmed as EEC by professional pathologists using H&E-stained sections after hysterectomy.

This study complied with all relevant ethical guidelines and was approved by the Medical Ethics Committee of the Affiliated Obstetrics and Gynecology Hospital of Nanjing Medical University (Approval No. [2021]KY-010). Prior to enrollment in the study, all patients were thoroughly informed about the use of their samples and provided written informed consent.

Preparation of human EEC tissues

The surgically resected EEC tumor tissues and peritumoral tissues were minced into small pieces (< 1 mm^3) on ice. These tissue fragments were then enzymatically digested using the GEXSCOPE Tissue Dissociation Mix (Singleron) under constant agitation for 30 minutes at 37°C. The single-cell solution was filtered through a 40 μm cell strainer to remove larger debris. Red blood cells were lysed using the GEXSCOPE Red Blood Cell Lysis Buffer (Singleron). Each sample was deemed qualified based on the following criteria: cell viability > 85%, total cell count > 1500, and red blood cells and impurities constituting < 20% of the sample.

Single-cell RNA sequencing and quality control of the scRNA-seq data

The single-cell suspensions were diluted to a concentration of $2×10^5$ cells/mL in phosphate-buffered saline (PBS, HyClone) and then loaded onto microfluidic devices. Subsequently, scRNA-seq libraries were generated using the GEXSCOPE Single-Cell RNA Library Kit (Singleron) following the manufacturer's standard protocol. This workflow encompassed barcoding, cDNA synthesis, and library construction. Each library was then diluted to a concentration of 4 mM and pooled for sequencing. The pooled library was sequenced on the NovaSeq 6000 platform (Illumina) using 150 bp paired-end reads. The raw scRNA-seq reads were processed to generate gene expression matrices using the CeleScope (v1.1.0) pipeline. Initially, low-quality reads, poly-A tails, and adapter sequences were trimmed using Cutadapt (v1.17) within the CeleScope pipeline. The cell barcode and UMI were extracted from the processed reads.

Afterward, reads were aligned to the GRCh38 reference genome (Ensembl version 92 annotation) using STAR (v2.6.1b). UMI and gene counts for each cell were quantified using featureCounts (v2.0.1), and utilized to generate expression matrix files for subsequent analysis. Cells were filtered based on the following criteria: gene counts < 200, the top 2% of gene counts and the top 2% of UMI counts. Cells with a greater than 20% mitochondrial content were removed. After quality filtering, 64 482 cells from 9 subjects were retained for downstream analyses.

Dimension-reduction and clustering

Dimensionality reduction and clustering were performed using functions from the Seurat package (v3.1.2). Normalization and scaling of the gene expression data were conducted using the NormalizeData and ScaleData functions, respectively. The most informative genes were identified using the FindVariableFeatures, selecting the top 2 000 variable genes for subsequent principal component analysis (PCA). Based on the top 20 principal components from PCA, cells were separated into distinct clusters with the FindClusters function. Finally, the uniform manifold approximation and projection (UMAP) algorithm was utilized to visualize the cells in two-dimensional space, providing a comprehensive representation of the cellular landscape.

Differentially expressed genes (DEGs) analysis

The Seurat FindMarkers function was employed to identify DEGs utilizing the Wilcox likelihood-ratio test with the default parameters. Genes expressed in more than 10% of cells within a cluster and exhibiting an average log (fold change) value > 0.25 were specifically selected as DEGs. During the analysis, doublet cells, characterized by co-expression of markers from distinct cell types, were manually identified and excluded.

Cell type annotation

The cell type identity of each cluster was determined based on the expression of canonical markers among the DEGs via the SynEcoSys database. The specific markers used for each cell type were as follows: for epithelial cells, KRT7, KRT17, and KRT19; for cancer cells, KRT8, KRT18, and EPCAM; for macrophages, CD163, C1QA, MRC1, MSR1, and APOE; for monocytes, CD14, FCN1, and VCAN; for dendritic cells, CD1C, IRF7, and CD14; for fibroblasts, DCN, COL1A1, and COL3A1; for T cells, CD3D, NKG7, and IL7R; for plasma cells, CD79A, and JCHAIN; for endothelial cells, PECAM1, CLDN5, and VWF; and for pericyte cells, ACTA2, RGS5, and MCAM. The top 6 genes, ranked based on their average fold-changes within each subcluster, were selected as the high-expression gene signature for that particular subcluster.

Copy number variation analysis

We utilized inferCNV to investigate the copy number variations among epithelial cells from both tumor and peritumoral tissues of EEC patients. This tool enables the estimation of somatic alterations in large-scale chromosomal copy number variants (such as amplifications or deletions) at the single-cell level. The epithelial cell raw single-cell gene expression data were extracted from the Seurat object according to the software manual. Single-cell data from immune cells and normal epithelial cells were used as reference controls, and inferCNV analysis was conducted using default parameters.

Gene set variation analysis (GSVA)

GSVA is a nonparametric and unsupervised algorithm designed to evaluate relative pathway activities in malignant epithelial cells. This analysis provided insights into the overall pathway activities within the cell population of interest.

UCell gene set scoring

Gene set enrichment scoring was performed using the UCell R package (v1.1.0). UCell scores are based on the Mann-Whitney U statistic by ranking query genes base on their expression levels in individual cells. As a rank-based scoring method, UCell is suitable for use in large datasets containing multiple samples and batches.

Cell cycle analysis

The cell cycle score of each cell was calculated using the CellCycleScoring function implemented in the Seurat package (v3.1.2).

Cell stemness analysis

We employed the SLICE package (v0.99.0) to assess the differentiation states within the three subtypes. SLICE encompasses two key functions: measuring cell differentiation states by calculating single-cell entropy (scEntropy) and predicting cell differentiation lineages by reconstructing trajectories based on scEntropy-derived differentiation states.

Pseudo time trajectory analysis: Monocle2

We analyzed the dynamic transcriptomic changes within the three subtypes and predicted the future transcriptional states of individual cell subtypes, using the Monocle2 package (v2.10.0). The top 2 000 highly variable genes were selected by Seurat (v3.1.2) FindVariableFeatures, and dimensionality reduction was performed using DDRTree to construct the trajectory. The trajectory was visualized with the plot cell trajectory function in Monocle2.

Transcription factor regulatory network analysis (pySCENIC)

A transcription factor (TF) network was constructed with pySCENIC (v0.11.0) using the scRNA expression matrix and transcription factors in AnimalTFDB. GRNBoost2 was employed to predict a regulatory network based on the co-expression of regulators and targets. CisTarget was then applied to exclude indirect targets and to search transcription factor binding motifs. Afterward, AUCell was used to quantify regulon activity in individual cell. Cluster-specific TF regulons were identified according to Regulon Specificity Scores (RSSs) and the activities of these TF regulons were visualized in heatmaps.

Cell-cell interaction analysis

The analysis of cell-cell interactions was conducted using CellPhoneDB (v2.1.0), which focuses on the known receptor-ligand interactions between two specific cell types. Cluster labels for all cells were

randomly permuted 1000 times to establish a null distribution, allowing for the calculation of the average expression levels of ligand-receptor pairs among interacting clusters. The expression levels of individual ligands or receptors were thresholded using a cutoff value determined by the average log gene expression distribution across all cell types. Cell-cell interactions were considered significant if they had a *P*-value < 0.05 and an average log expression > 0.1, and these interactions were visualized using the circlize (v0.4.10) R package.

KEGG and GO analysis

We employed the clusterProfiler (v3.16.1) R package to perform Gene Ontology (GO) and Kyoto Encyclopedia of Genes and Genomes (KEGG) analyses to explore the possible functions of the DEGs. Significant enrichment of pathways was determined based on *P* value < 0.05. Reference gene sets from GO were utilized, encompassing the molecular function (MF), biological process (BP), and cellular component (CC) categories.

Gene set score combined with an analysis of clinical factors

Bulk RNA-seq transcriptome data and clinical information were obtained from TCGA database. The relationships between the target gene set and clinical factors were evaluated using GSEA and GSVA to calculate a score for each gene set in each sample, and the samples were subsequently assigned to two groups (high group and low group) using the median score as the cutoff. Differences in overall survival between the high and low groups were compared using Kaplan-Meier survival curves, with *P*-values calculated via the log-rank test using the survival package in R.

Tissue microarray (TMA) and immunohistochemistry (IHC)

IHC staining of the TMA was performed with the labeled-avidin-biotin technique. The TMA were incubated with antibodies specific for AREG (Abmart, #MK00655M, 1:200) and PAX-2 (Abmart, #T55212M, 1:200). IHC staining of AREG and PAX-2 in the tissue was evaluated using the semiquantitative H score, independently by two pathologists who were blinded to the clinical data. Staining intensity was categorized into 4 grades: 0 (no staining), 1 (weak staining), 2 (moderate staining), and 3 (strong staining). The H score was calculated by multiplying the staining intensity score by the percentage of cells exhibiting that intensity level. The scores for each intensity grade were summed to yield the final H score. The H score (ranging from0 to 300) was calculated using the formula: H score = 3 × (% of cells with score 3) + 2 × (% of cells with score 2) + 1 × (% of cells with score 1).

EEC cell lines and cell culture

The EEC cell lines (HEC-1-A, ISHIKAWA, MFE 296, and AN3 CA) as well as the human normal endometrial epithelial cells (HNEECs) were obtained from the American Type Culture Collection. EEC cells and HNEECs were cultured separately in DMEM or DMEM F12 (Gibco, Carlsbad, CA, USA), supplemented with 10% fetal bovine serum (FBS) (Vivacell, Shanghai, China) and 1% penicillin/streptomycin (Gibco, Carlsbad, CA, USA). All cell lines were incubated at 37°C in a 5% CO_2 environment. Regular testing was

conducted to detect any mycoplasma contamination. All cell lines were authenticated to confirm their identity.

Construction of stably overexpressing and knockdown cell lines via transfection

The packaging plasmids (psPAX2 and pMD2.G) were co-transfected with the core plasmids into HEK293T cells to produce recombinant virus particles. ISHIKAWA and AN3 CA cells (2×10^5 cells per well in a six-well plate) were transfected with a lentivirus in serum-free medium, followed by replacement with complete medium after 12 hours. Cells were selected using puromycin (2 μg/mL) for two weeks to ensure stable transduction.

RNA extraction and RT-qPCR analysis

Total RNA was extracted from the cells using the FastPure Cell/Tissue Total RNA Isolation Kit V2 (Vazyme). Reverse transcription was performed using the HiScript II Q RT SuperMix for qPCR (Vazyme) to synthesize complementary DNA (cDNA) from RNA. Quantitative PCR (qPCR) was conducted using ChamQ SYBR qPCR Master Mix (without ROX) (Vazyme). The mRNA expression levels of each gene were normalized to the reference gene GAPDH. The sequences of primers used for RT-qPCR was listed in S Table 3.

Western blot

Protein preparation and WB were performed according to standard protocols. Primary antibodies against AREG (Abcam Cat# ab89119, 1:1000) and GAPDH (Proteintech Cat# 60004-1-Ig, 1:100000) were used. HRP-conjugated goat anti-rabbit IgG (Bioworld Cat# BS13278, 1:10000) and goat anti-mouse IgG (Bioworld Cat# BS12478, 1:10000) were used as secondary antibodies. The blots were developed using the an ECL kit for WB(Vazyme). The blots were exposed to X-ray film, which was subsequently scanned using a Tanon 4800 Multi Photo Scanner.

Flow cytometry

EEC cells were incubated with surface antibodies specifically targeting AREG (Thermo Fisher Cat# 25-5370-42, 5 μl/test) in PBS for 30 minutes at room temperature to examine AREG expression. Following two washes with PBS, the cells were analyzed using a flow cytometer (CytoFLEX, Beckman Coulter, Shanghai, China) within 1 hour.

CCK8, colony formation, and EdU assays

For the CCK8 assay, cells were seeded in 96-well plates at a density of 1×10^3 cells per well. After an incubation for 4 days, the CCK8 assay (Vazyme) was performed. The optical density (OD) was measured at 450 nm using a multifunction microplate reader (TECAN). For the colony formation assay, cells were seeded in 6-well plates at a density of 1.5×10^3 cells per well. The cell culture medium was changed every 3 days over a period of approximately 3 weeks. Colonies were fixed with 4% paraformaldehyde at

room temperature for 30 min, stained with 0.1% crystal violet for 30 minutes and then photographed. For the EdU assay, cells were seeded in 24-well plates at a density of 1×10^4 cells per well. The BeyoClick™ EdU Cell Proliferation Kit with Alexa Fluor 555 (Beyotime) was used in accordance with the manufacturer's instructions.

Transwell assay

We used transwell chambers (Corning) with an 8 μm pore size filter and a Matrigel (Corning) coating for the invasion assay. For the migration assay, cells were cultured in serum-free DMEM for 12 hours. Then, 5×10^4 cells suspended in 200 μl of serum-free DMEM were added to the upper chamber of a 24-well plate. In the lower chamber, 800 μl of DMEM containing 20% FBS was added. After 48 hours of incubation, the migrated cells were fixed with 4% paraformaldehyde for 30 minutes and stained with 0.1% crystal violet for 30 minutes. The upper chamber was washed with water and non-migratedcells were carefully removed using cotton swabs. Images of the migrated cells in the upper chamber were then randomly captured using a microscope and counted using ImageJ software. For the invasion assay, 40 μl of diluted Matrigel was added to the upper chamber and allowed to solidify at 37°C for approximately 1 hour. The remaining steps were the same as those in the migration assay.

Wound healing assay

For the wound healing assay, cells were seeded in 6-well plates at a concentration of 1×10^6 cells per well. After an overnight incubation, a 200 μl pipette tip was used to make a straight wound with the aid of a straight edge. The cells were cultured in DMEM containing 1% FBS for 72 hours.

Cell cycle and apoptosis analysis

For cell cycle analysis, ISHIKAWA and AN3 CA cells were fixed with 70% ethanol at 4 ℃ and analyzed using a Cell Cycle Analysis Kit (YEASEN, Cat# 40301ES50, Shanghai, China) according to the manufacturer's protocol. For apoptosis analysis, cells suspended in PBS were stained with an Annexin V-Alexa Fluor 647/PI Apoptosis Detection Kit (YEASEN, Cat# 40304ES50, Shanghai, China). The stained cells were then analyzed using a flow cytometer (CytoFLEX, BECKMAN COULTER, Shanghai, China) equipped with FlowJo software for the analysis of the cell cycle distribution and apoptosis distribution.

Construction of xenograft tumor models in BALB/c nude mice

Forty 4-week-old female BALB/c nude mice were obtained from the Animal Core Facility of Nanjing Medical University. These mice were maintained under specific pathogen-free conditions and all procedures were conducted in compliance with protocols approved by the Institutional Animal Care and Use Committee of Nanjing Medical University. For the xenograft model, female BALB/c nude mice were randomly classified into four groups: ISHIKAWA-sh-Control, ISHIKAWA-sh-AREG, AN3 CA-AREG-VE, and AN3 CA-AREG-OE (n = 6 per group). ISHIKAWA-shNC (3×10^6), ISHIKAWA-shAREG (3×10^6), AN3 CA-AREG-VE (5×10^6), and AN3 CA-AREG-OE (5×10^6) cells were suspended in 200 μL of serum-free DMEM and

injected subcutaneously into the dorsal region of the mice. Tumor volume was measured weekly using Vernier calipers. After three weeks, the mice were euthanized and the tumors were excised for further analysis. Tumor volume and weight were measured to assess the effects of the different treatments. The tumors were fixed with 4% paraformaldehyde at 4°C for subsequent H&E and IF staining. IF staining was performed to visualize the expression of the Ki-67 and AREG proteins.

Statistical Analysis

Data are presented as the means ± standard deviation (SD), unless specified otherwise. IBM SPSS Statistics 25, GraphPad Prism 9.0.0 and R software 3.5.1 were used to analyze the data and plot the graphs. Student's t test, one-way analysis of variance, or the chi-square test was used to analyze differences. Overall survival (OS) was defined as the duration from the date of surgery to death for any reason. Kaplan—Meier curves were used to plot OS curves, and the log-rank test was used to evaluate differences in survival. Statistical significance was defined as $P < 0.05$. $P < 0.05$, $P < 0.01$, $P < 0.001$, and $P < 0.0001$ are indicated by *, **, ***, and ****, respectively.

Abbreviations

EC: endometrial cancer; EEC: endometrioid endometrial cancer; TCGA: The Cancer Genome Atlas; CNV: copy number alteration; TME: tumor microenvironment; scRNA-seq: single-cell RNA sequencing; GSVA: gene set variation analysis; EMT: epithelial-mesenchymal transition; TF: transcription factor; DCs: dendritic cells; EGFR: epidermal growth factor receptor; HCC: hepatocellular carcinoma; TMA: tissue microarrays; IHC: immunohistochemical; H&E: haematoxylin and eosin; AEH: atypical endometrial hyperplasia; qPCR: quantitative polymerase chain reaction; WB: western blot; FCM: flow cytometry; EdU: 5-ethynyl-2' -deoxyuridine; CCK-8: cell counting kit-8; IF: immunofluorescence; pro-CD8-Teff cells: Proliferating CD8 effector T cells; CD8-Teff cells: CD8 effector T cells; CD4-Treg cells: CD4 regulatory T cells; CD4-Tfh cells: CD4 follicular helper T cells; NK cells: Natural killer cells; AML: acute myeloid leukemia; PBS: phosphate-buffered saline; PCA: principal component analysis; DEGs: differentially expressed genes; GO: Gene Ontology; KEGG: Kyoto Encyclopedia of Genes and Genomes; MF: molecular function; BP: biological process; CC: cellular component; HNEEC: human normal endometrial epithelial cells; FBS: fetal bovine serum; OD: optical density; OS: overall survival; UMAP: uniform manifold approximation and projection.

Declarations

Acknowledgment

The authors thank the patients who participated in this study, as well as the Nanjing Maternity and Child Health Care Hospital and the National Health Commission Key Laboratory of Antibody Techniques for providing the research platform for this study.

Funding Statement

This study is supported by the grants from the Jiangsu Provincial Medical Youth Talent (QNRC2016104) and the Science and Technology Support Program of Jiangsu Province (BE2018613).

Competing interests

All authors declare no financial or non-financial competing interests.

Author Contributions

QWW and TSN were responsible for collecting the clinical specimens.QWW and HYT were major contributors in writing the manuscript. HYX and HXT and SHB have made significant contributions in the field of data processing. FT and CXX and XHZ and TYF reviewed and revised the manuscript. TQ and FZQ and GY oversaw the design of the project. ZHL provided financial support and clinical samples.

References

1. Sung, Hyuna et al. Global Cancer Statistics 2020: GLOBOCAN Estimates of Incidence and Mortality Worldwide for 36 Cancers in 185 Countries. CA Cancer J Clin. 71,3 (2021): 209–249.
2. Makker, Vicky et al. Endometrial cancer, Nat Rev Dis Primers 7(1) (2021) 88.
3. R.L. Siegel, K.D. Miller, H.E. Fuchs, A. Jemal, Cancer statistics, 2022, CA Cancer J Clin 72(1) (2022) 7–33.
4. R. Murali, R.A. Soslow, B. Weigelt, Classification of endometrial carcinoma: more than two types, Lancet Oncol 15(7) (2014) e268-e278.
5. Cancer Genome Atlas Research Network et al. Integrated genomic characterization of endometrial carcinoma, Nature 497(7447) (2013) 67–73.
6. Dou, Yongchao et al. Proteogenomic Characterization of Endometrial Carcinoma, Cell 180(4) (2020) 729–748.e26.
7. Tang, Fuchou et al. mRNA-Seq whole-transcriptome analysis of a single cell, Nat Methods 6(5) (2009) 377–82.
8. Wu, Liang et al. An invasive zone in human liver cancer identified by Stereo-seq promotes hepatocyte–tumor cell crosstalk, local immunosuppression and tumor progression, Cell Research 33(8) (2023) 585–603.
9. Cheng, Chao et al. Immune Infiltration in Tumor and Adjacent Non-Neoplastic Regions Codetermines Patient Clinical Outcomes in Early-Stage Lung Cancer, Journal of Thoracic Oncology 18(9) (2023) 1184–1198.
10. Bersuker, Kirill et al. The CoQ oxidoreductase FSP1 acts parallel to GPX4 to inhibit ferroptosis, Nature 575(7784) (2019) 688–692.
11. Balsa, Eduardo et al. NDUFA4 Is a Subunit of Complex IV of the Mammalian Electron Transport Chain, Cell Metabolism 16(3) (2012) 378–386.

12. Dunlap, Sarah M et al. Insulin-like growth factor binding protein 2 promotes glioma development and progression, Proc Natl Acad Sci U S A 104(28) (2007) 11736–11741.
13. Rani, Aradhana et al. HES1 in immunity and cancer, Cytokine & Growth Factor Reviews 30 (2016) 113–117.
14. Chang, Yu-Chan et al. Regorafenib inhibits epithelial-mesenchymal transition and suppresses cholangiocarcinoma metastasis via YAP1-AREG axis, Cell Death Dis 13(4) (2022).
15. L. Uusküla-Reimand, M.D. Wilson, Untangling the roles of TOP2A and TOP2B in transcription and cancer, Sci Adv 8(44) (2022) eadd4920.
16. Uxa, Sigrid et al. Ki-67 gene expression, Cell Death & Differentiation 28(12) (2021) 3357–3370.
17. Islam, Ridwan et al. Role of Neuropilin-2-mediated signaling axis in cancer progression and therapy resistance, Cancer and Metastasis Reviews 41(3) (2022) 771–787.
18. C. Dong, L. Zhao, X. Liu, L. Dang, X. Zhang, Single-cell analysis reveals landscape of endometrial cancer response to estrogen and identification of early diagnostic markers, PLoS One 19(3) (2024) e0301128.
19. Ren, Fang et al. Single-cell transcriptome profiles the heterogeneity of tumor cells and microenvironments for different pathological endometrial cancer and identifies specific sensitive drugs, Cell Death Dis 15(8) (2024) 571.
20. Ren, Xiaojun et al. Single-cell transcriptomic analysis highlights origin and pathological process of human endometrioid endometrial carcinoma, Nat Commun 13(1) (2022) 6300.
21. Yu, Xinnian et al. Integrating single-cell RNA-seq and spatial transcriptomics reveals MDK-NCL dependent immunosuppressive environment in endometrial carcinoma, Front Immunol 14 (2023) 1145300.
22. Yu, Zhicheng et al. Single-cell sequencing reveals the heterogeneity and intratumoral crosstalk in human endometrial cancer, Cell Prolif 55(6) (2022) e13249.
23. Liu, Yang et al. Overview of AKR1C3: Inhibitor Achievements and Disease Insights, Journal of Medicinal Chemistry 63(20) (2020) 11305–11329.
24. Eun, Jung Woo et al. Cancer-associated fibroblast-derived secreted phosphoprotein 1 contributes to resistance of hepatocellular carcinoma to sorafenib and lenvatinib, Cancer Communications 43(4) (2023) 455–479.
25. Chi, Yudan et al. Cancer cells deploy lipocalin-2 to collect limiting iron in leptomeningeal metastasis, Science 369(6501) (2020) 276–282.
26. Chen, Ziyang et al. OLFM4 deficiency delays the progression of colitis to colorectal cancer by abrogating PMN-MDSCs recruitment, Oncogene 41(22) (2022) 3131–3150.
27. Castillo, Josefa et al. Amphiregulin contributes to the transformed phenotype of human hepatocellular carcinoma cells, Cancer Res 66(12) (2006) 6129–38.
28. Yotsumoto, Fusanori et al. Amphiregulin regulates the activation of ERK and Akt through epidermal growth factor receptor and HER3 signals involved in the progression of pancreatic cancer, Cancer

Science 101(11) (2010) 2351–60.
29. Hsu, Ya-Ling et al. Lung tumor-associated dendritic cell-derived amphiregulin increased cancer progression, Journal of Immunology 187(4) (2011) 1733–44.
30. Jiang, Jiajia et al. Over expression of amphiregulin promoted malignant progression in gastric cancer, Pathology - Research and Practice 215(10) (2019) 152576.
31. Weng, Hengyou et al. The m6A reader IGF2BP2 regulates glutamine metabolism and represents a therapeutic target in acute myeloid leukemia, Cancer Cell 40(12) (2022) 1566–1582.e10.
32. T. Liu, X. Wang, J. Zhai, Q. Wang, B. Zhang, Long Noncoding RNA UCA1 Facilitates Endometrial Cancer Development by Regulating KLF5 and RXFP1 Gene Expressions, Cancer Biother Radiopharm 36(6) (2021) 521–533.
33. Roy, Sohini et al. Macrophage-Derived Neuropilin-2 Exhibits Novel Tumor-Promoting Functions, Cancer Res 78(19) (2018) 5600–5617.
34. Zhou, Yanming et al. ZEB1 enhances Warburg effect to facilitate tumorigenesis and metastasis of HCC by transcriptionally activating PFKM, Theranostics 11(12) (2021) 5926–5938.
35. Zhang, Ming et al. FOSL1 promotes metastasis of head and neck squamous cell carcinoma through super-enhancer-driven transcription program, Mol Ther 29(8) (2021) 2583–2600.
36. Watzling, Martin et al. Three-Dimensional Breast Cancer Model to Investigate CCL5/CCR1 Expression Mediated by Direct Contact between Breast Cancer Cells and Adipose-Derived Stromal Cells or Adipocytes, Cancers (Basel) 15(13) (2023).
37. Cheng, Tsu-Yao et al. Annexin A1 is associated with gastric cancer survival and promotes gastric cancer cell invasiveness through the formyl peptide receptor/extracellular signal-regulated kinase/integrin beta-1-binding protein 1 pathway, Cancer 118(23) (2012) 5757–5767.
38. P.S. Filippou, G.S. Karagiannis, A. Constantinidou, Midkine (MDK) growth factor: a key player in cancer progression and a promising therapeutic target, Oncogene 39(10) (2020) 2040–2054.
39. Yu, Xinnian et al. Integrating single-cell RNA-seq and spatial transcriptomics reveals MDK-NCL dependent immunosuppressive environment in endometrial carcinoma, Frontiers in Immunology 14 (2023).
40. Zhang, Yijian et al. Single-cell RNA-sequencing atlas reveals an MDK-dependent immunosuppressive environment in ErbB pathway-mutated gallbladder cancer, J Hepatol 75(5) (2021) 1128–1141.
41. Jeong, Bo Young et al. Lysophosphatidic acid-induced amphiregulin secretion by cancer-associated fibroblasts augments cancer cell invasion, Cancer Lett 551 (2022) 215946.
42. N.M. Monte, K.A. Webster, D. Neuberg, G.R. Dressler, G.L. Mutter, Joint Loss of PAX2 and PTEN Expression in Endometrial Precancers and Cancer, Cancer Res 70(15) (2010) 6225–6232.
43. Bertero, Alessandro et al. The SMAD2/3 interactome reveals that TGFβ controls m6A mRNA methylation in pluripotency, Nature 555(7695) (2018) 256–259.
44. A. Dongre, R.A. Weinberg, New insights into the mechanisms of epithelial–mesenchymal transition and implications for cancer, Nature Reviews Molecular Cell Biology 20(2) (2018) 69–84.

45. Mucciolo, Gianluca et al. EGFR-activated myofibroblasts promote metastasis of pancreatic cancer, Cancer Cell 42(1) (2024) 101–118 e11.

Figures

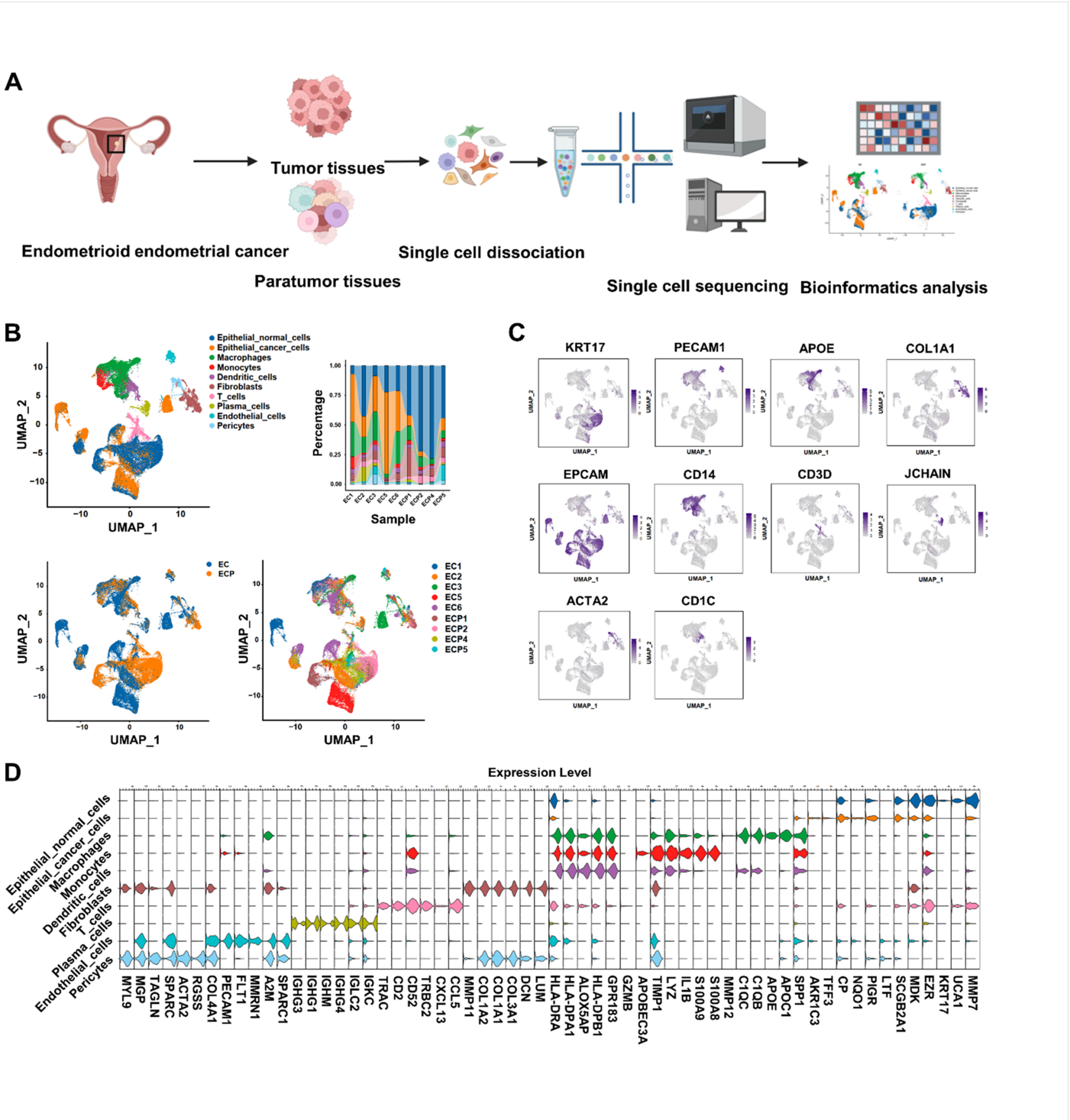


Figure 1

Cellular atlas of EEC and peritumoral tissues. (A) Schematic diagram of the generation of the scRNA-seq data. EECs and peritumoral tissues were dissociated into single cells, and sequenced using the 10×

Genomics platform for further bioinformatics analysis. (B) Uniform manifold approximation and projection (UMAP) plot for the identification of different clusters of single cells in EECs, including normal epithelial cells (n=24,025; KRT17), epithelial cancer cells (n=15,965; EPCAM), macrophages (n=9,778; APOE), monocytes (n=2,038; CD14), dendritic cells (n=2,154; CD1C), fibroblasts (n=4,295; COL1A1), T cells (n=2,042; CD3D), plasma cells (n=1,751; JCHAIN), endothelial cells (n=1,252; PECAM1), and pericytes (n=1,182; ACTA2). UMAP plots of EEC and peritumoral cells split by sample and region. Sankey diagram of the proportions of different cell types in the 9 samples. (C) Feature plots showing the specific cell marker genes of different cell types. (D) Violin plots showing the top 6 DEGs of different cell types. "EC" refers to samples from tumor tissues and "ECP" refers to samples from peritumoral tissues.

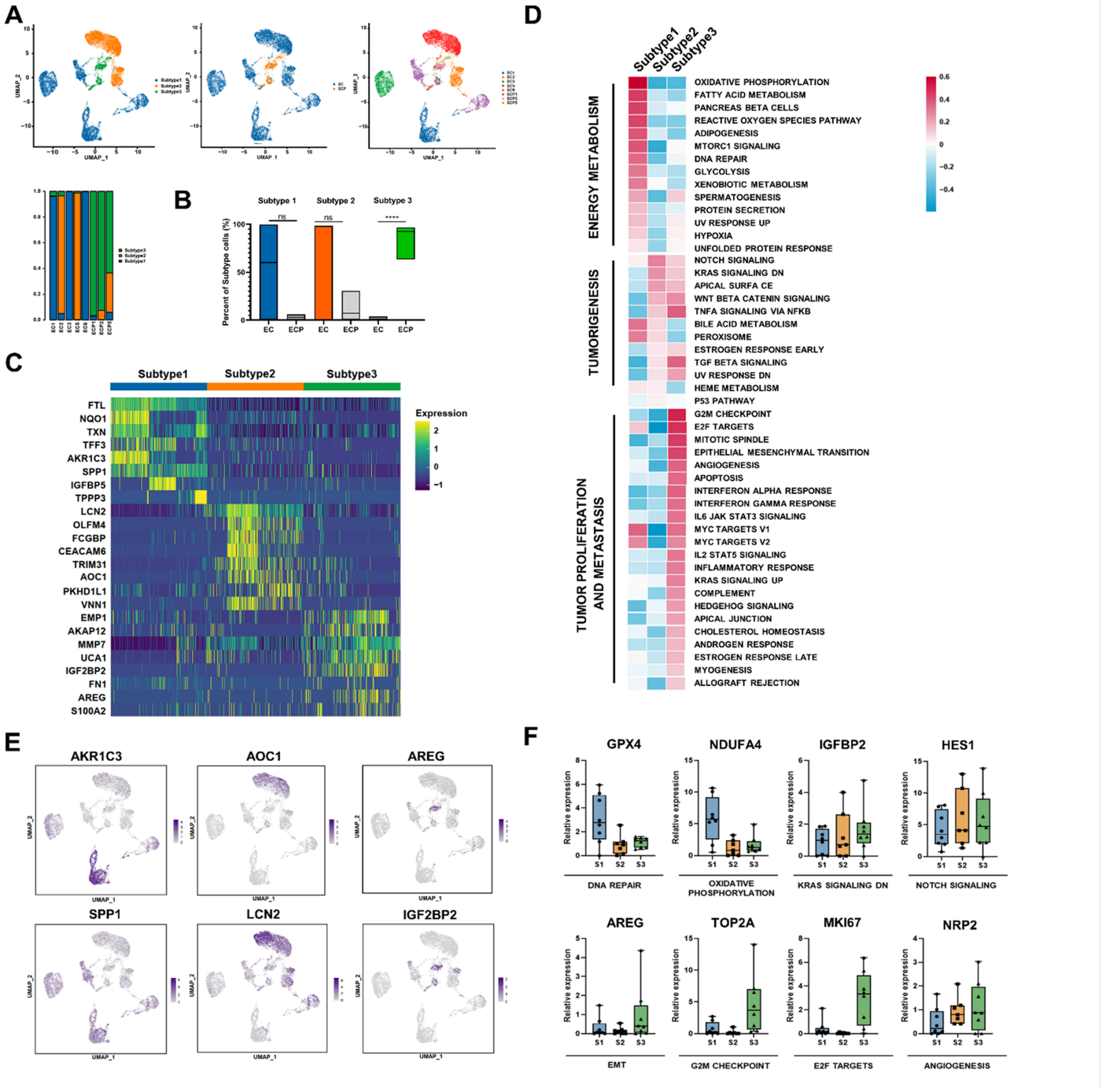


Figure 2

Distinct features of epithelial cancer cells in EEC and peritumoral tissues. (A) UMAP plot for the identification of the three subtypes of malignant epithelial cells. UMAP plots of the three subtypes split by sample and region. Bar plot showing the proportions of the three subtypes in the 9 samples. (B) Percentages of the three subtypes in tumor and peritumoral tissues. Student's t test, ****$P < 0.0001$. (C) Heatmap showing the top 8 DEGs among the three subtypes. (D) GSVA showing enriched pathways associated with each subtype of malignant epithelial cells. (E) Feature plots showing the specific cell marker genes of the three subtypes. (F) Bar plots showing the relative expression of classical genes corresponding to the gene sets in the three subtypes.

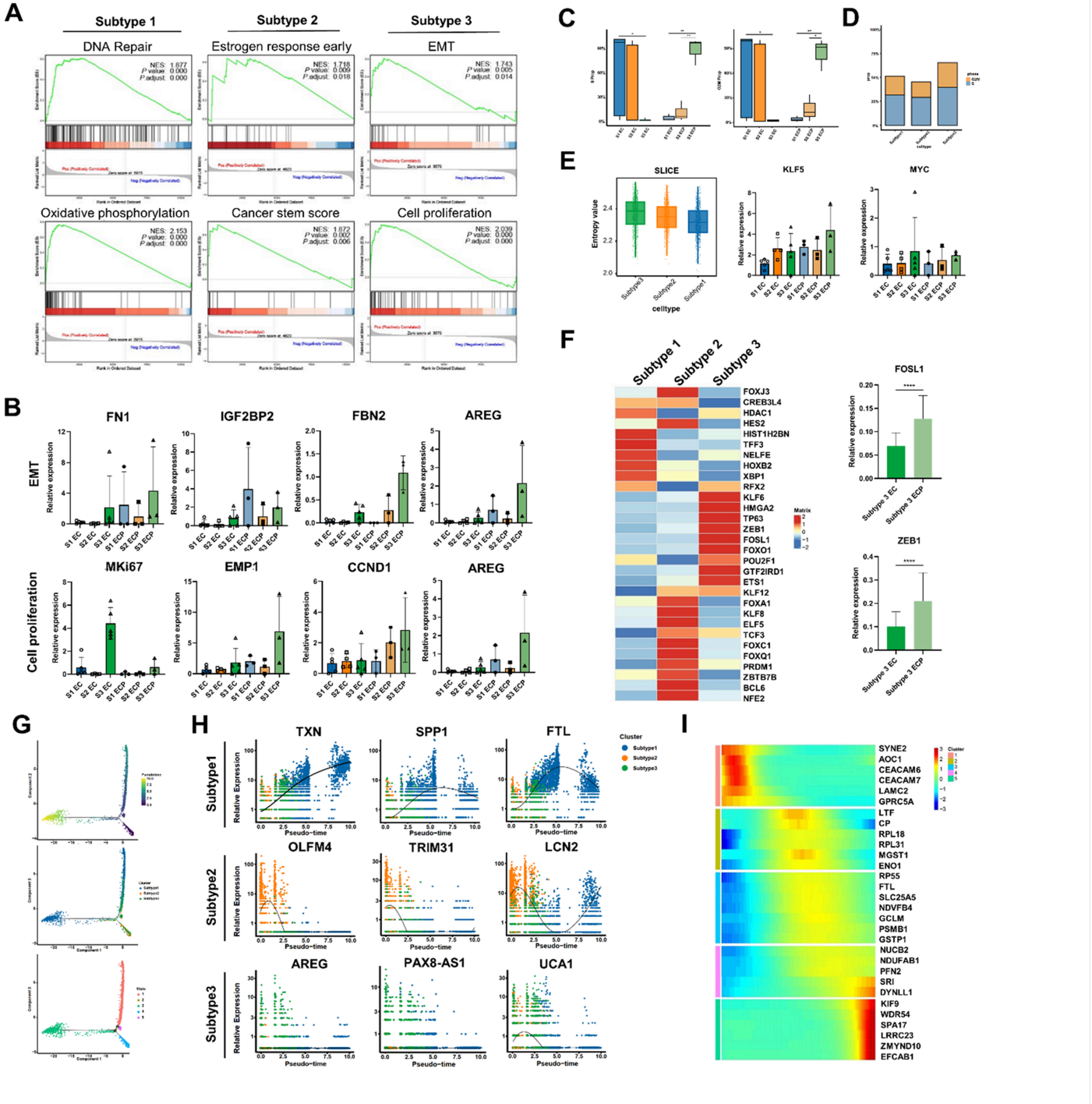


Figure 3

Functional identification and analysis of the AREG^{+} S3 cell population. (A) Significantly identified pathways enriched in the three subtypes. S1 had significantly high enrichment scores for the DNA repair and oxidative phosphorylation gene sets. S2 exhibited notable enrichment scores for the estrogen response early and cancer stemness score gene sets. S3 showed remarkable enrichment scores for the EMT and cell proliferation gene sets. (B) The relative expression levels of cell proliferation-related genes (MKI67, AREG, EMP1, and CCND1) and EMT-related genes (FN1, AREG, IGF2BP2, and FBN2) in the three

subtypes (EC/ECP). (C) Boxplots comparing the ratios of three subtypes of malignant cells (EC/ECP) in S and G2M phases are shown. Wilcoxon rank-sum test, *P < 0.05 and **P < 0.01. (D) The bar plot shows the percentage of cells in S and G2M phases in the three subtypes. (E) Boxplots comparing the entropy values of the three subtypes. Wilcoxon rank-sum test, ****P < 0.0001. The relative expression levels of the stemness-related genes KLF5 and MYC in the three subtypes (EC/ECP). (F) The heatmap shows the top 10 differentially expressed transcription factors among the three subtypes. The bar plot shows the relative expression of FOSL1 and ZEB1 in S3 EC/ECP. Student's t test, ****P < 0.0001. (G) The developmental pseudotime trajectories of the three subtypes inferred via analysis with Monocle2. The color key from dark to bright indicates cancer progression from the early to the late stage. (H) Node gene expression along the differential trajectories. (I) Heatmap displaying the significantly differentially expressed genes during the progression of EEC. The color key from blue to red indicates the relative expression levels from low to high.

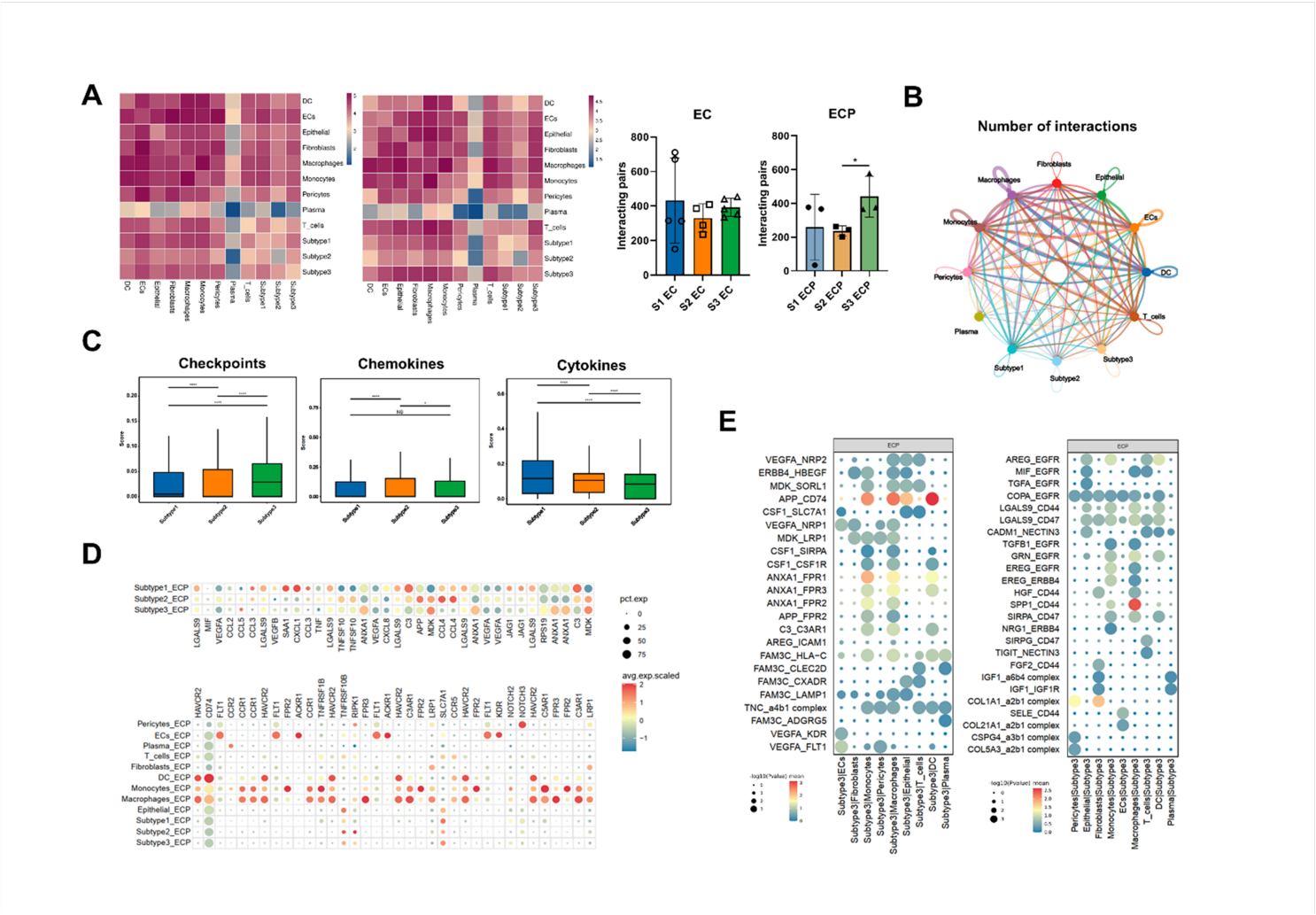


Figure 4

Cell-cell communication between the three subtypes and other cell types. (A) The heatmap shows the strength of potential ligand–receptor interactions between three subtypes and nine other cell types predicted by CellPhoneDB. The bar plot shows the number of interacting pairs between three subtypes (EC/ECP) and nine other cell types. Student's t test, *P< 0.05. (B) Circus plot describing the interactions

between three subtypes and nine other cell types. (C) Bar plot displaying the checkpoint scores, chemokine scores, and cytokine scores of the three subtypes. Student's t test, *$P < 0.05$, ****$P < 0.0001$. (D) Crosstalk between the three subtypes and other cell types in peritumoral regions. Top panel: Differentially expressed ligands of tumor cells in each subtype. Bottom panel: Respective receptors and their expression by cell type. (E) The dot plot depicts the interacting pairs formed by the ligand and receptor respectively. Dot sizes and colors refer to the intensity of cells expressing the receptor and ligand, respectively.

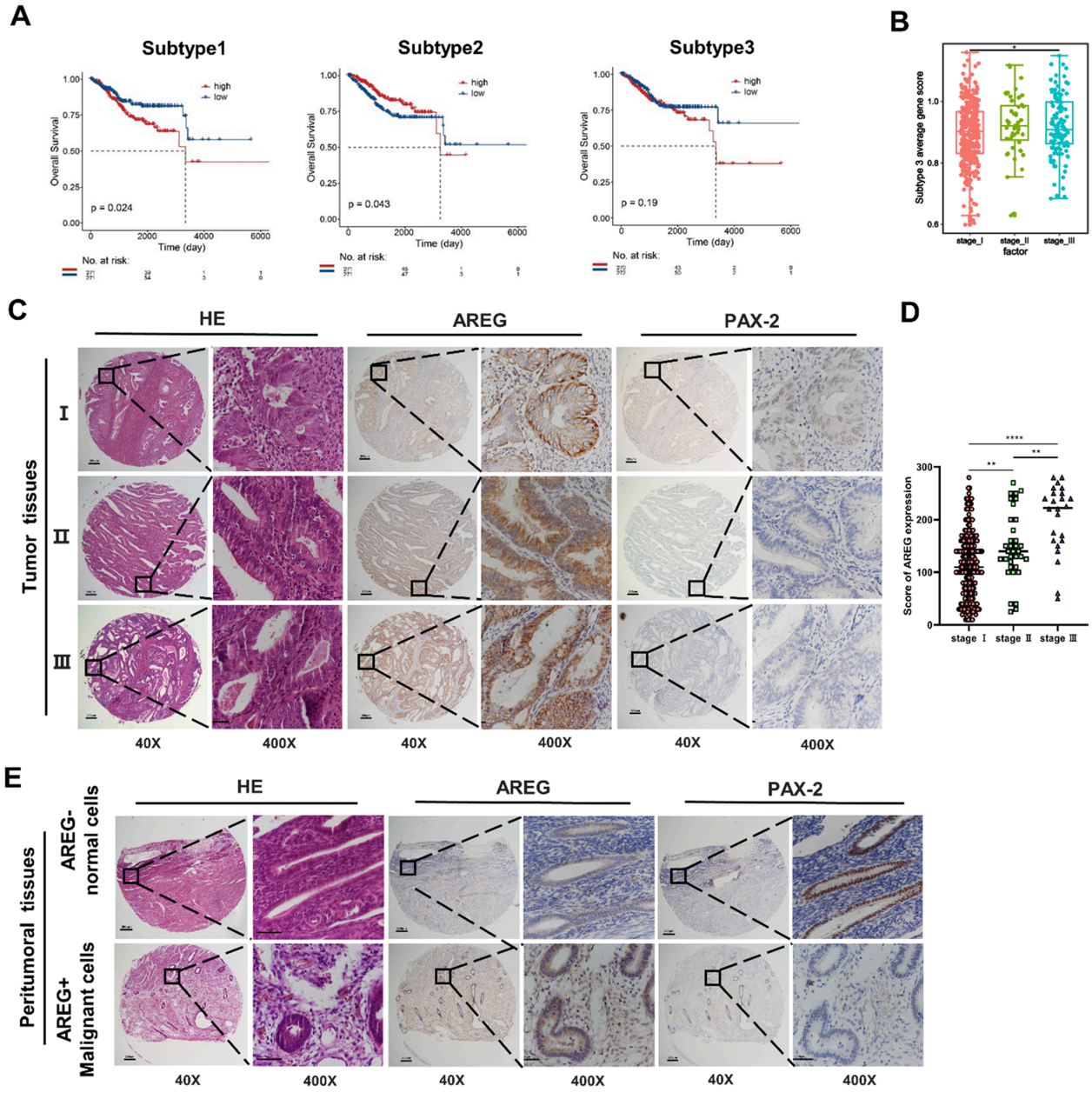


Figure 5

Expression of AREG in EEC tissues and peritumoral tissues and its relationship with clinicopathological factors and prognosis. (A) OS curves based on TCGA-EEC database (n = 542 patients), with patients stratified by average expression (binary: high versus low) of the S1-S3 gene set. Survival curves were compared via the log–rank test and visualized using the Kaplan–Meier method. (B) Box plot displaying the variations in the S3 average gene score in EEC stages I-III. Student's t test, *$P < 0.05$. (C) Hematoxylin and eosin (H&E) staining of EEC tissues (stages I-III) and IHC staining for the AREG and PAX-2 proteins in EEC tissues (stages I-III). Representative micrographs are shown at the original magnification (×400). Scale bars, 50 μm. (D) Dot plot showing the total IHC score for AREG in different EEC stages (n = 296). Student's t test, **$P < 0.01$ and ****$P < 0.0001$. (E) H&E staining of EEC peritumoral tissues and IHC staining for the AREG and PAX-2 proteins in EEC peritumoral tissues. Representative micrographs are shown at the original magnification (×400). Scale bars, 50 μm.

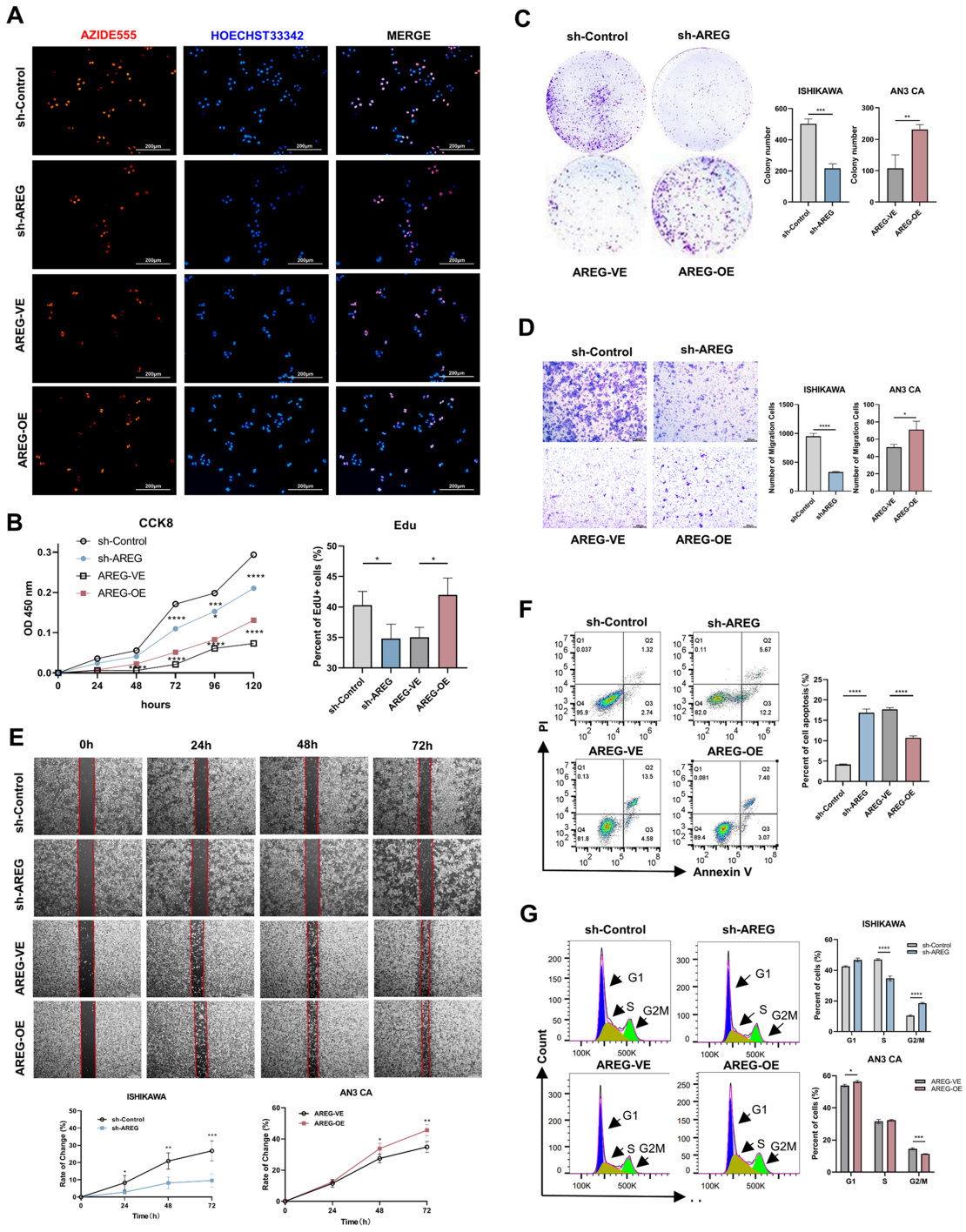


Figure 6

Effects of AREG on the biological behaviors of EEC cells*in vitro*. (A) An EdU assay was performed to assess the proliferation ability of AREG-knockdown cells (ISHIKAWA) and AREG-overexpressing cells (AN3 CA). Scale bars, 200 μm. (B) Left: A CCK8 assay was used to measure the proliferation ability of AREG-knockdown cells (ISHIKAWA) and AREG-overexpressing cells (AN3 CA) at 0 h, 24 h, 48 h, 72 h, 96 h, and 120 h. Right: Statistical results of EdU assay. (C) Colony formation assays were conducted to

evaluate the proliferation ability of AREG-knockdown cells (ISHIKAWA) and AREG-overexpressing cells (AN3 CA). (D) Transwell assays were used to assess the migration capacity of AREG-knockdown cells (ISHIKAWA) and AREG-overexpressing cells (AN3 CA). (E) Wound healing assays were used to measure the migration capacity of AREG-knockdown cells (ISHIKAWA) and AREG-overexpressing cells (AN3 CA) at 0 h, 24 h, 48 h, and 72 h. (F) Annexin V-Alexa Fluor 647/PI staining was performed to analyze the percentages of apoptotic AREG-knockdown cells (ISHIKAWA) and AREG-overexpressing cells (AN3 CA), and the results are displayed in bar plots. (G) FCM was used to analyze the cell cycle of AREG-knockdown cells (ISHIKAWA) and AREG-overexpressing cells (AN3 CA), and the populations of cells in G1, S, and G2/M phases are shown in bar plots. The data are shown as the means ± SDs. Student's t test, $*P < 0.05$, $**P < 0.01$, $***P < 0.001$, and $****P < 0.0001$.

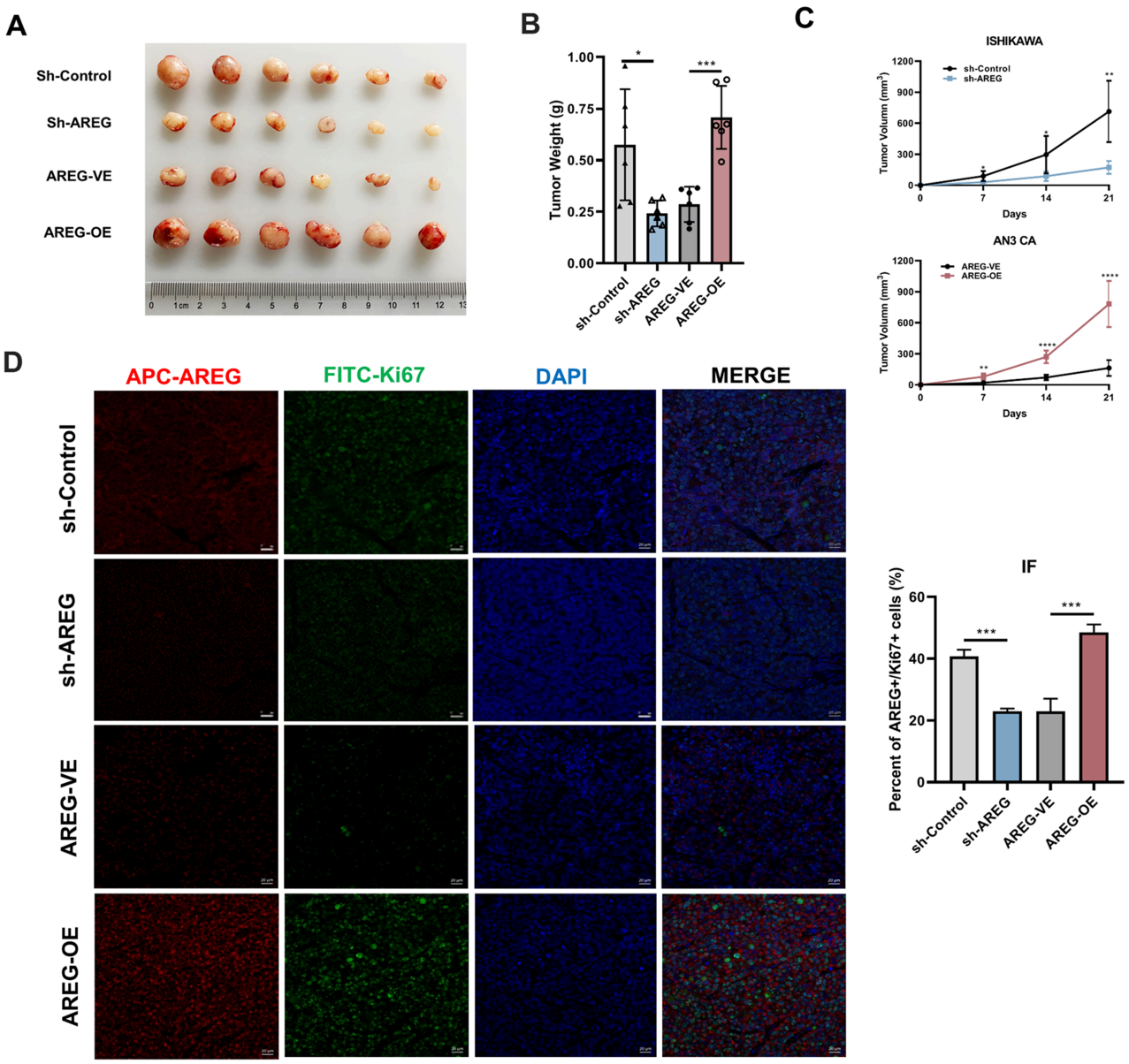


Figure 7

Effect of AREG on EEC cell proliferation *in vivo*. (A) Photographs of tumors (ISHIKAWA, AN3 CA) removed from the mouse subcutaneous xenograft model. (B) Bar plot showing the weights of the tumors. (C) Line graphs depicting the change in the volume of tumors in the knockdown and overexpression groups over a three-week period. (D) IF staining was performed to identify AREG^{+} (red), Ki67^{+} (green), and Hoechst 33342-stained (blue) cells to assess the proliferation of EECs. The bar plot displays the number of colocalized cells (AREG^{+}, Ki67^{+}) in the knockdown and overexpression groups. Scale bar, 20 μm. The data are shown as the means ± SDs. Student's t test, **P* < 0.05, ***P* < 0.01, ****P* < 0.001, and *****P* < 0.0001.

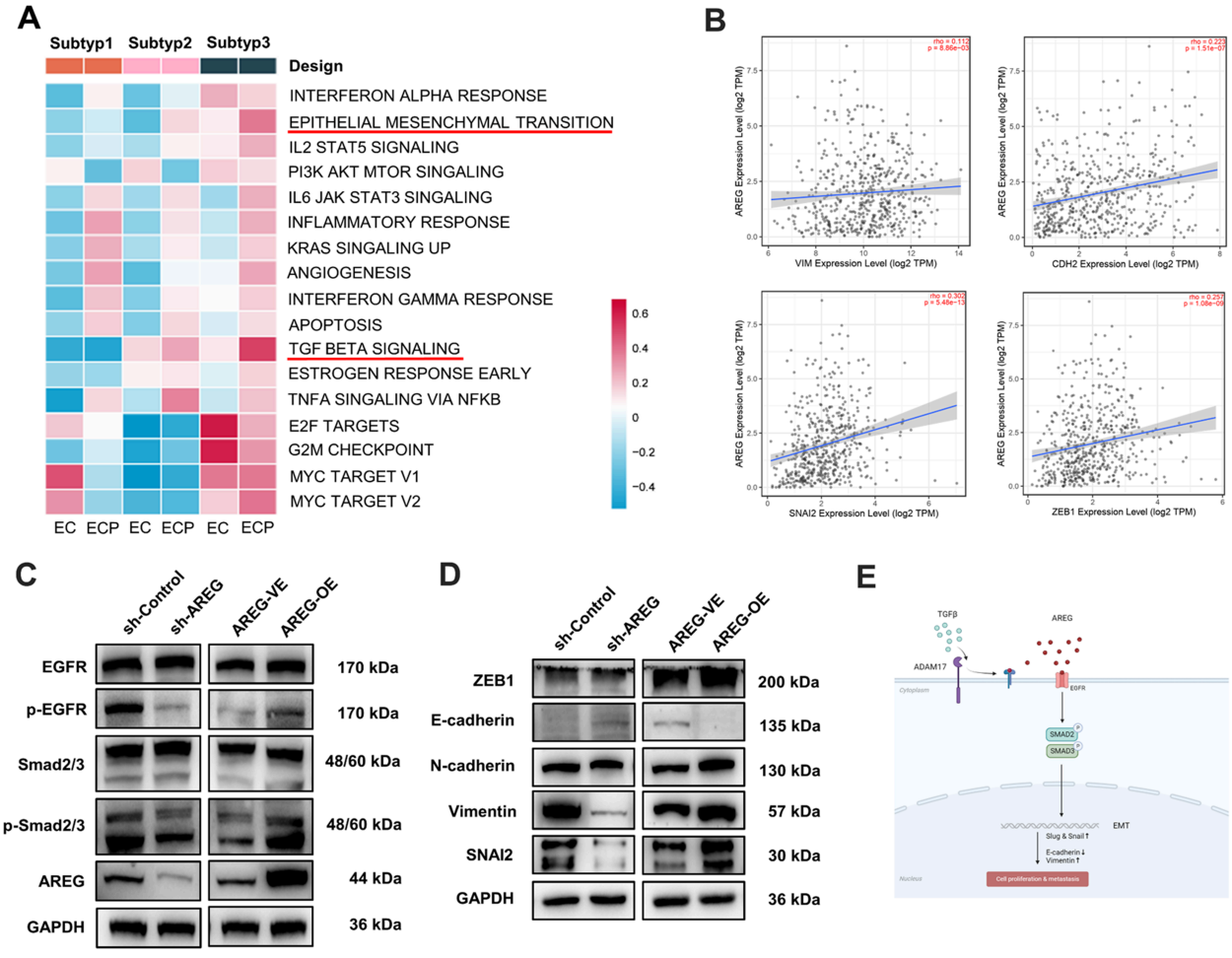


Figure 8

AREG induced the EMT via EGFR-Smad2/3 signaling to promote the migration and invasion of EEC cells. (A) GSVA showing the enriched pathways of malignant epithelial cells in S1-S3 EC/ECP. (B) Pearson's

correlation analysis was performed to assess the associations between the expression levels of EMT-related genes (VIM, CDH2, SNAI2, and ZEB1) and AREG from the TIMER 2.0 Database. (C) The protein levels of EGFR, p-EGFR, Smad2/3, p-Smad2/3 and AREG were detected by WB in AREG-knockdown cells (ISHIKAWA) and AREG-overexpressing cells (AN3 CA). (D) ZEB1, E-cadherin, N-cadherin, vimentin, and SNAI2 protein levels were detected by WB in AREG-knockdown cells (ISHIKAWA) and AREG-overexpressing cells (AN3 CA). (E) Schematic illustration showing that AREG induced the EMT via EGFR-Smad2/3 signaling to promote EEC metastasis.

Supplementary Files

This is a list of supplementary files associated with this preprint. Click to download.

- SupplementaryTable1.docx
- SupplementaryTable2.docx
- SupplementaryTable3.docx
- SupplementaryTable4.docx
- ECsupplementaryFig1.tif
- ECsupplementaryFig2.tif
- ECsupplementaryFig3.tif
- ECsupplementaryFig4.tif
- ECsupplementaryFig5.tif